Visible-induced photocatalytic reactivity of polymer-sensitized titania nanotube films

Hai-chao Liang, Xiang-zhong Li*

Department of Civil and Structural Engineering, The Hong Kong Polytechnic University, Hunghom, Kowloon, Hong Kong, China

Tel.: +852 2766 4113; fax: +852 2334 6379.

[*] E-mail address: cexzli@polyu.edu.hk

Abstract

In this study, polythiophene-TiO_2 nanotube films (PTh/TNT) were successfully prepared by a two-step electrochemical process of anodizaton and electropolymerization, in which a highly-ordered TiO_2 nanotube (TNT) film was anodized at a low-voltage with post calcination first and then the prepared TNT film was deposited with a polythiophene layer by electropolymerization in the BFEE electrolyte. The morphology and structures of PTh/TNT composites were examined by FESEM, EDX, XRD, and XPS methods. XPS spectra of PTh/TNT composites indicate the strong interaction between S sites of polymer backbone and TiO_2 nanotubes, in which electron transfer from polythiophene to titania takes place. UV-vis DRS analysis shows that these composites have a strong photoresponse in the visible region at 500 nm. The prepared PTh/TNT films revealed significant activity for 2,3-DCP degradation under visible light irradiation and also sunlight irradiation, in which the PTh3/TNT film achieved the best performance. On the other hand, this study also confirmed that the side-chains of polythiophene could influence its photocatalytic activity significantly in an order from high to low as poly3-methylthiophene ≈ polythiophene > polythiophenecarboxylic acid > poly3-hexylthiophene. The results may provide useful information to further develop

some effective polymer-semiconductor catalysts for pollutant degradation under sunlight irradiation for water and wastewater treatment.

Keywords: Polymer; Photosensitizer; Titania nanotubes; Visible photocatalysis

1. Introduction

Solar energy conversion, water splitting, and the elimination of recalcitrant organic pollutants through visible light photocatalysis using TiO_2 nanotube films are of paramount interests. To let TiO_2 nanotubes as well as TiO_2 particles be active under visible light, various types of sensitizers including organic dyes [1,2], organometallic complexes [3], and inorganic quantum dots [4] can be attached onto the surface of TiO_2 nanotubes. Among these visible light sensitizers, $Ru(bpy)_3^{2+}$ and its derivatives, attributed to organic dyes, seem to be one of the most successful and widely used in solar cells [5,6]. However, such dye sensitizers are not sufficiently stable in the aquatic environment and need to be prepared only in the acidic pH region. Therefore, water splitting and elimination of recalcitrant organic pollutants using Ru-complex sensitized TiO_2 has not been very successful. It is necessary to exploit more novel visible-light-sensitized photocatalysts with uniform sizes and microstructures for the energy storage/conversion, water splitting, and environmental applications.

The conjugated polymers with extending π-conjugated electron systems such as polyaniline, polythiophene, polypyrrole, and their derivatives have shown great promises due to their high absorption coefficients in the visible part of the spectrum, high mobility of charge carriers, and excellent stability [7]. In general, they are also efficient electron donors and good hole transporters upon visible light excitation [8]. Recently, conjugated polymers act as stable photosensitizers combined with wide band gap inorganic semiconductors (e.g., TiO_2, ZnO, CdSe and CdTe) is an emerging area of research for optical, electronic, and photoelectric

conversion applications [9-11]. In a conjugated polymer/TiO_2 system, polymer, bound to TiO_2, can actively harvest the visible light matching the semiconductor energy levels, and then inject electrons into the conduction band (CB) of TiO_2. Over the past several decades, researchers have investigated the movement of charge across the bulk/molecular interfaces successfully, and have described them theoretically. A schematic diagram for the charge transfer processes of conjugated polymer and TiO_2 is illustrated in Fig. 1. Here, when the conjugated polymer harvests visible light, an absorbed photon promotes an electron from the ground state of the polymer located in the semiconductor energy gap into an excited state that is in resonance with the CB. The polymer π-orbital becomes the highest occupied molecular orbital (HOMO) in the combined system. Since the lowest unoccupied molecular orbital (LUMO) levels of polymer are energetically higher than the conduction band edge of TiO_2 [12, 13], the electron transfer paths in Fig. 1 are possible. Efficient electron injection into the edge of the CB avoids the energy loss by relaxation to the CB edge [14]. The injected electron delocalizes from bulk to surface, simultaneously relaxing to the bottom of the CB owing to coupling to vibrations. If the electron remains trapped at the surface, it will react with the electron acceptor such as oxygen or hydrogen peroxide residing on the electrolyte mediator. As a result, it should be a vital prerequisite for photosensitization that the interfacial charge transfer between photosensitizer and semiconductor takes place, being capable of responding to visible light. However, there are quite limited reports to gain attention to the photocatalysis of TiO_2 sensitized by such a polymer under visible light irradiation.

[Fig. 1]

Polythiophene and its derivatives, a kind of sulfur-containing conjugated polymer, are photochemically and thermally stable under photoirradiation, which have been often used as sensitizers in polymer-sensitized TiO_2 photovoltaic devices [15,16]. Furthermore, they have

also been used as catalysts to degrade organic pollutants in the environment [17]. Besides, it is interesting that the polythiophene and its derivatives do not undergo degradation under UV radiation in the presence of TiO_2, which has been confirmed by lots of literatures [17-19]. In present study, we therefore chose polythiophene as a photosensitizer to be attached on the anodic TiO_2 nanotube films through an electropolymerization technique and thereby investigated the photocatalytic reactivity of polythiophene-TiO_2 composites under visible light irradiation. The roles of polythiophene layers on TiO_2 nanotubes and the effects of various factors on the sensitized photoactivity were also studied with details. This study is aimed at utilizing the ability of polymer sensitization by visible light and providing better understanding of the mediated electron-transfer process and interactive oxidation reaction of the functionalized polymer/TiO_2 composites.

2. Experimental

2.1. Chemicals and materials

2,3-dichloropgenols (2,3-DCP), thiophene, boron fluoride-ethyl ether (BFEE), and ammonium fluoride (NH_4F) were purchased from Aldrich Chemical Company and used without further purification. Titanium foils (140 μm thickness, 99.6% purity) were purchased from Goodfellow Cambridge Ltd. Other chemicals were obtained as analytical grade reagents. Deionized distilled (DD) water was used throughout the experiments.

2.2. Synthesis of anodic TiO_2 nanotube arrays

A large piece of raw Ti foil was cut into small rectangle pieces (1.0 cm × 3.0 cm each), which were ultrasonically cleaned in an acetone-ethanol solution and then washed with DD water. An anodic oxidation process was conducted in a dual-electrode reaction chamber, in which the cleaned Ti foil was used as the anode and a Pt foil of the same size was applied as

the cathode. Two electrodes with a distance of 2 cm were submerged into 0.1 M NH_4F electrolyte solution at pH 1.5 adjusted with H_2SO_4 and an direct current power supply (EPS 600) was used to provide an electrical potential of 25 V between two electrodes during the anodic oxidation reaction. The resulting TiO_2 nanotubular films on Ti substrate were then rinsed by DD water and subsequently calcined at 500 ^oC for 1 h (named "TNT").

2.3. Synthesis of polythiophene-sensitized TNT composites

An electrochemical polymerization process was employed to prepare the polythiophene-sensitized TNT composites in a one-compartment cell, in which the prepared TNT film as the anode and a Pt sheet (1 cm × 4 cm) as the cathode (a counter electrode) were immersed in the BFEE electrolyte solution, while a saturated calomel electrode (SCE) was also used as the reference electrode. Three electrodes were connected with a potentiostat-galavanostat (ZF-9 ZhengFang Company, Shanghai). The working and counter electrodes were placed 1.0 cm apart. The electrolyte solution consists of fresh BFEE and various amounts of thiophene as request, where BFEE furnishes the conducting medium [20]. The electrolyte solution was deoxygenated by bubbling nitrogen gas before the electrochemical polymerization.

A polythiophene layer was gradually coated on the TNT film by the electrochemical polymerization process at 1.3 V (vs. SCE) potentiostatically for 1 min. This low potential avoids any degradation of the polymer and any side reactions between the electrolytes and electrodes due to the occurrence of overoxidation at 1.45–1.55 V [21]. The thickness of polythiophene layer was controlled by the concentrations of thiophene monomers (1, 3, and 5 mM) in the BFEE electrolyte solution, corresponding to three composites named "PTh1/TNT", "PTh3/TNT", and "PTh5/TNT", respectively. All the resulting composite films were washed repeatedly with diethyl ether and DD water, and then dried at 80 ^oC under vacuum for 6 h before characterization. For comparison, a polythiophene film was also

prepared by depositing polythiophene onto an optical ITO-glass electrode instead of on the TNT film by electrochemical polymerization in the BFEE electrolyte solution with a thiophene concentration of 5 mM at 1.3 V for 1 min and was named "PTh/ITO".

2.4. Characterization

The surface morphology of resulting samples was studied by field-emission scanning electron microscopy (FESEM; JSM6300, Japan) and elemental analysis was performed with energy dispersive X-ray (EDX) spectroscopy. Information on the chemical states of the as-prepared samples was obtained from X-ray photoelectron spectroscopy (XPS, SKL-12). XPS measurements were also carried out with a twin anode (Al/Mg) X-ray source and a charge neutralizer. All the binding energies were referenced to the C 1s peak at 284.6 eV of the surface adventitious carbon. A UV–visible spectrophotometer (Perkin Elmer, Lambda 20) was used to directly record the diffuse reflectance spectra (DRS) of resulting photocatalysts. Baseline correction was done using a calibrated sample of barium sulphate. The concentration of dissolved organic carbon (DOC) in aqueous solution was determined using a total organic carbon analyzer (TOC-5000A, Shimadzu, Japan).

2.5. Photoactivity measurement

The experiments of 2,3-DCP degradation in aqueous solution were performed in a single-compartment photoreactor equipped with a TNT or PTh/TNT film. A 150-W high pressure sodium lamp, positioned inside a cylindral circulating water jacket (Pyrex), was employed as an external visible light source. The lamp mainly provides visible light in the range of 400-800 nm, as reported in our previous publication [22]. A light filter containing 1.0 M aqueous $NaNO_2$ solution was placed inside the Pyrex jacket to completely eliminate any UV radiation at a cutoff wavelength of 400 nm. The as-prepared catalyst film with an area of 3 cm^2 was

placed in 25 mL of aqueous 2,3-DCP solution with an initial concentration of 20 mg L^{-1}; prior to photoreaction, the aqueous mixture was magnetically stirred in the dark for 60 min to reach adsorption/desorption equilibrium; then the reaction solution with stirring was irradiated by the visible light; during the photoreaction, samples were collected at different time intervals for analysis. The 2,3-DCP concentration was determined by HPLC (Finnigan SpectraSYSTEM P4000) consisting of a Pinnacle II C18 reverse-phase column (5 μm, 4.6 mm × 250 mm) and a UV detector (UV 6000LP). A mobile phase was composed of acetonitrile and water (v:v = 3:2) and flowed at 1.0 mL min^{-1}. In all solar experiments, the whole set-up was placed under sunlight irradiation on April 16, 2008 from 9:00 a.m. to 4:00 p.m. with an average solar intensity of 401 W m^{-2}.

3. Results and discussion

3.1. Morphology and elemental composition

The morphology and elemental composition of as-formed TNT and PTh/TNT films were first examined by FESEM and EDX analyses and the results are shown in Fig. 2. From the SEM image of TNT film in Fig. 2a1, it can clearly be observed that the highly ordered and perforated porous TNT arrays with a wall-thickness of ~12 nm and a tube length of ~350 nm are well formed on the Ti substrate. When viewed from an angle perpendicular to the surface, the TNT arrays appear to be highly-uniform tubular and their tube mouths are open and smooth. The EDX spectrum of the TNT film in Fig. 2a2 showed two signals of Ti (K_α and K_β) at 4.51 and 4.93 keV, respectively, and also two additional signals of a L_α peak of Ti and a K_α peak of O at 0.53 KeV. Besides the above peaks, no peaks representing other elements were detected in the EDX analysis and XPS spectra (not shown here). These results indicate that the anodic TNT films prepared in this study consisted of Ti and O only, but no other elements

such as N, F, or S existing in the electrolyte solution were doped into the lattice of TiO_2 in this low-voltage anodization process.

[Fig. 2]

Fig. 2b-d shows the SEM images and EDX spectra of PTh1/TNT, PTh3/TNT, and PTh5/TNT composites, respectively. It was observed that unlike the pure TNT film, the polythiophene layer formed on TNT substrate yielded the rough pore mouth and also some disordered aggregates on the wall surface of the TNT arrays (b1). Comparing three composites (PTh1/TNT, PTh3/TNT and PTh5/TNT), it can be found that the higher strength of thiophene in the electrolyte BFEE solution formed the thicker polythiophene layer with its extension to the top and inner wall of TiO_2 nanotubes (see c1 and d1). This phenomenon might result from the higher current density through the electrolyte solution, since a fixed potential was applied at 1.3 V (vs. SCE). Current-time response curves for the polymerization of thiophene at different monomer concentrations are shown in Fig. 3. These curves demonstrated a same pattern that current density varied violently at the initial time and gradually stabilized to approach a plateau, which is similar to other earlier reports [23,24]. It can be seen that the stabilized current density was higher with the higher concentration of monomer (5 mM). The relevant behaviors for the current as a function of time have been described in metal deposition [25].

During the electropolymerization of thiophene, the dissolved species of monomer or short oligomers are first transferred to radical cations and two radical cations can combine together to form an unstable dehydrogenated dication, which then released protons to form a longer oligomer chain (see Scheme 1). In this case, the electrodeposition of polythiophene is similar to that of metal deposition mentioned above, in which it proceeds through a nucleation and growth pathway. This mechanism has been confirmed by Hillman's group using potentiostatic steps [23]. Their data indicated that a bulk film was formed by the instantaneous nucleation

and three-dimensional growth of polymer on top of this monolayer. Rate constants for growth parallel to the surface on substrate and the covering polymer layer were very close. Within a narrow potential range, the observation of maxima and minima in current-time transients was interpreted in terms of the "death" and "rebirth" of growing centers. Through layer-by-layer deposition, therefore, it is possible to manufacture films with a thickness of limited number of monolayers which may find important and useful technology.

[Fig. 3]

[Scheme 1]

EDX analysis revealed the chemical composition of the three PTh/TNT composites (PTh1/TNT, PTh3/TNT, and PTh5/TNT) as shown in Fig. 2 (b2, c2, and d2), respectively. Similar to the TNT sample, the three composites exhibit the strong K diffraction peaks at 4.51, 4.92, and 0.52 keV, corresponding to the elemental Ti and O, respectively. At the same time, two new diffraction peaks at 0.28 and 2.31 keV also appeared in their EDX spectra, corresponding to the elemental C and S. An approximate ratio of S/Ti was estimated for each sample, according to the integral areas of the characteristic peaks for both elements. The spectra indicate that the ratios of S/Ti in the three PTh/TNT composites are approximately 0.1, 0.8, and 13.3 wt %, respectively. These results therefore reflect the feasibility of the chemical modification of polythiophene molecules for nanotubular TiO_2 films, and the amount of polythiophene coated is significantly dependent on the concentration of monomer used in the electrolyte solution.

3.2. XRD and XPS characterization

The XRD patterns of the Ti foil, TNT, PTh1/TNT, PTh3/TNT, and PTh5/TNT samples are shown in Fig. 4. The pure TNT calcined at 500 ^{o}C had characteristic peaks at 25.35^{o} (101), 27.5^{o} (110), 36.1^{o} (101), 48.1^{o} (200), 54.3^{o} (211), and 69.8^{o} (220), which are in good

agreement with previous reports [26,27]. According to the indexation of peaks, the TNT film calcined at 500 ^{o}C thus mainly contains anatase and rutile phases. For the PTh1/TNT composite, it can be seen that the peak intensity of rutile quickly decreases and the anatase peak at $2\theta = 25.35^{o}$ becomes smaller and broader compared to that of the TNT film. A more critical trend can be confirmed for the two samples of PTh3/TNT and PTh5/TNT as with the increased amount of polythiophene, the diffraction peak of anatase (101) became smaller and broader, and peaks attributed to rutile phase (110) disappeared completely. This probably because the amorphous state of the polythiophene polymer deposited on/in TNT attenuated the characteristic diffraction of TNT, thus affecting the detection of the crystal diffraction of TNT film. As a result, it should be noted that the presence of polythiophene has a significant effect on the TiO_2 crystalline structure observed in the pure TNT film.

[Fig. 4]

Table 1 shows the binding energies of S 2p and Ti 2p obtained from their high resolution XPS spectra. Obviously, the binding energies of S 2p for the pure polythiophene film (peeled off from the PTh/ITO samples) can be deconvoluted into three peaks (Fig. 5a) centered at 163.32, 164.41 and 167.57 eV. The first two peaks are assigned to the neutral S $2p_{3/2}$, and the oxidized S $2p_{1/2}$. With these results it is possible to quantitatively separate the oxidized thiophene sulfur species from total thiophene sulfur species according to the areas of two sulfur peaks. In the pure PTh sample, about 45% fraction of thiophene contain the oxidized sulfur. The third peak (at 167.57 eV) is associated with the formation of positively charged sulfur ($S^{\delta+}$) [28]. This positive charge is consistent with the formation and transport of polarons and bipolarons in the conductive grafted polythiophene chains. However, its content in total thiophene sulfur species is only about 6%, much less compared to the first two peaks. This result indicates that the neutral and oxidized sulfur species were mainly produced in the polymer backbone when thiophene monomer was electropolymerized at 1.3 V for 1 min. The

XPS peaks of S 2p in PTh3/TNT (Fig. 5b) can also be deconvoluted into three peaks as well as that of the polythiophene film, while the higher binding energy (163.69, 164.89 and 168.28 eV) is observed. This result indicates the strong interaction between polythiophene and titania through electron transfer from polythiophene to titania, or the formation of bonding between sulfur and oxygen [28]. While the PTh3/TNT and PTh5/TNT composites showed a similar pattern of their composition, the PTh5/TNT composite showed a higher ratio of S/Ti and also a higher level of the positively charged sulfur. In contrast, a small shift to the lower value of the Ti 2p binding energies of three composites occurs as compared to that of the TNT sample. This also reflects the strong interaction between S sites of polymer backbone and TiO_2 nanotubes, in which electron transfer from polythiophene to titania takes place. From the results of FESEM, XRD, and XPS analyses, it can be confirmed that the PTh/TNT composites were successfully formed by this two-step electrochemical process.

[Table 1]

[Fig. 5]

3.3. Optical properties

The optical properties of the as-prepared samples were studied by measuring their UV-vis absorption. Fig. 6 shows the UV-vis absorption spectra of PTh, TNT, and PTh/TNT composites, where the as-prepared PTh/ITO sample was placed in the reference beam to measure the UV-vis absorption of PTh film. The spectrum of PTh/ITO (curve a) shows a broad absorption band from 350 to 650 nm with its maximum absorption at ~500 nm, which is attributed to π-π* (HOMO-LUMO) transition of the polythiophene backbones. It has been reported that the large π-conjugated systems of polythiophene can create small π-π* energy gaps within the visible spectrum [29]. The width of absorption band indicates the coexistence of both long and short effective conjugation lengths in the polythiophene chains.

The TNT sample (curve b) in Fig. 6 shows very weak absorption in the visible region with its band gap transition starting from ~395 nm. This is attributed to the unique tubular structures of TiO_2. Unlike TNT, the PTh/TNT composites (curves c-e) in Fig. 6 exhibit a new and broad absorption band in the range of 400–600 nm with a main shoulder at 540 nm. These results further imply the existence of the interaction between polymer and nanotubular TiO_2, as identified by the XPS spectra. Moreover, this pattern becomes more prominent with an increased amount of polythiophene layers (curves c-e). Obviously, the TNT film functionalized with polythiophene causes a strong red shift in its light absorption as a result of the strong electronic interaction between polythiophene and titania and a direct charge transfer from polythiophene to the semiconductor surface that takes place during the photoexcitation. A transition of energy levels between this polymer orbital and TiO_2 orbital, as shown in Fig. 1 would be a key step to result in such as a significant red shift.

[Fig. 6]

3.4. Photocatalytic activity under visible light irradiation

The photocatalytic activity of PTh/TNT composites was evaluated in terms of the 2,3-DCP degradation in aqueous solution under visible light irradiation and the TNT sample was also tested for comparison, as shown in Fig. 7. It is found that only a minor removal of 2,3-DCP either under visible illumination only or with TNT under visible illumination after 420 min reaction. These results therefore indicate that the direct photolysis and the TNT photocatalysis did not demonstrate any significant photoactivity under visible illumination. In contrast, the 2,3-DCP was significantly degraded by 51% using the PTh3/TNT composite under visible illumination after 420 min reaction and, at least four different intermediates from 2,3-DCP degradation were detected by HPLC. In a polymer-TiO_2/visible light system, some positive carbon radicals in polymer chains are formed, as well as in a dye sensitized-TiO_2 system,

when the photoexcited electrons of polythiophene are injected into the conduction band of TiO_2. These positive carbon radicals undergo delocalization along the conjugated π-orbital on polymer chains until to be attacked by an electronegative group. When the electronegative group is water or oxygen, the resulting molecule may be called a hydrogen radical or triplet/singlet oxygen [30], respectively, which is an active oxidizer and is capable of attacking organic pollutants to the ultimate products. Therefore, 2,3-DCP may be degraded through one or more pathways. The study of intermediates and pathways was not conducted in this paper and it would be an interesting point for a further study using the GC-MS or NMR analysis.

Fig. 7b shows the visible photoactivity of three PTh/TNT composites in our experiment. It can be seen that the PTh3/TNT sample exhibits the highest photocatalytic activity by 51% of 2,3-DCP removal after 420 min irradiation, while the PTh1/TNT and PTh5/TNT degraded 2,3-DCP by 42% and 34%, respectively under the same experimental condition. This result indicates there is an optimal amount of the polythiophene deposition to achieve the best photocatalytic performance. Actually, the optical properties of PTh/TNT composites depend on the growth mechanism of the polythiophene layer during electrochemical synthesis. When a very low concentration of thiophene monomer (e.g., less than 1 mM) was applied, the detached polymer clusters were yielded on the TNT substrate, as shown in Fig. 2b1. As a result, only a small fraction of photons are absorbed by the detached polymer clusters to sensitize TiO_2 nanotubes crystal, leading to the limited photocatalytic activity. In contrast, with an increased concentration of thiophene monomers in the electrolyte solution, more polymer chains were aggregated and a well-connected polythiophene layer was formed on the TNT substrate surface (see Fig. 2c1 and d1). These well-connected polythiophene films can provide more photos to carry out the charge transfer on the PTh/TNT interface, resulting in the higher photocatalytic activity. However, the fact is that the photoactivity of PTh/TNT with

an excessively thick polythiophene layer such as PTh5/TNT declined in the experiments, which might be attributed to the combination of three factors, including (1) the reduced active surface area of TNT films, (2) the poor pore structure (see the SEM images in Fig. 2), and (3) the occurrence of profuse defects (such as the formation of positively charged sulfur) in the deposited polymer chain.

[Fig. 7]

To evaluate the reusability of the PTh/TNT films, the PTh3/TNT film was repeatedly used for several experimental runs, in which each run lasted for 420 min. After the first photocatalytic reaction, the catalyst was rinsed by DD water, dried at 103 ^{o}C and re-used immediately without any treatment. The experimental results showed that after 5 runs the activity of PTh3/TNT film only decreased slightly to be ~86% of the photocatalytic efficiency in the first run, which indicates that the PTh3/TNT films can maintain relatively high activity.

3.5. Photocatalytic activity under UV light irradiation

One set of experiments for 2,3-DCP degradation under UV light irradiation was performed and the results are presented in Fig. 8. It is observed that the 2,3-DCP with an initial concentration of 20 mg L^{-1} was degraded by 78% under UV light irradiation for 300 min with the TNT sample, and by ~62% with the PTh3/TNT sample. It is easy to understand that, for the PTh3/TNT sample, both the polythiophene and TiO_2 can be excited by UV light irradiation. The excited electrons on the CB of TiO_2 will accumulate and resist any electrons transfer from the photoexcited states of polythiophene. Consequently, the electrons on the CB of TiO_2 either delocalize inside TiO_2 bulk or eventually find its way to transfer into the ground state of polymer [14]. Moreover, the coating of polythiophene not only lowers down the extent of TNT crystallinity (see XRD spectrum in Fig. 4), but also reduces the active surface area of TNT. Therefore, the overall photocatalytic efficiency of PTh/TNT was lower

than that of TNT under UV illumination. This observation is similar to the general fact that the modification of TiO_2 to achieve visible photoactivity always looses its photocatalytic activity under UV light to a certain extent as reported by the earlier studies [31,32].

[Fig. 8]

3.6. Photocatalytic activity under sunlight irradiation

As utilizing sunlight is always the most economical option to conduct photoreaction [33,34], this composite PTh/TNT film should be photocatalytically active under sunlight irradiation with a broad wavelength range from near UV to visible region. It is worth to extend the above experiments to be conducted outdoor under sunlight irradiation to further revaluate the photocatalytic activity of the PTh/TNT catalyst.

Fig. 9 shows the degradation of 2,3-DCP by TNT and PTh3/TNT films under sunlight irradiation. It can be clearly found that the 2,3-DCP degradation with the PTh3/TNT film was achieved by about 88% after 420 min reaction, while that with TNT film was only by 70%. To explain these results, the optical behavior of the composite materials under solar illumination must be considered. It is well known that sunlight not only contains visible light but even UV light (< 5% of the total radiation) passing through the atmosphere to the earth. The experimental results in Fig. 9 showed that 2,3-DCP degradation with the TNT film under sunlight irradiation was much more slowly than that with the PTh/TNT film, since sunlight has only a small fraction of UV light. These results indicate that the PTh/TNT catalyst can effectively absorb both of UV and visible lights to promote the electronic excitation between the valence and conduction bands, where the fraction of UV light is responsible for the well-known direct excitation of TiO_2 and visible light responds to the sensitized excitation. The two approaches can promote the generation of electro-hole pairs and also charge transfer through the interaction between PTh layer and TiO_2 nanotubes. It is generally accepted that if

the electrons and holes created do not recombine rapidly, they need to be either trapped in some metastable states or migrate to the semiconductor surface separately, in which the amount of surface-trapped carriers is responsive for determining the overall activity of the TiO_2 films [35]. Consequently, the sunlight experiments reveal the major contribution of the sensitization mechanism under UV-vis light rather than the direct excitation of TNT.

[Fig. 9]

To further evaluate the efficiency of various catalysts irradiated by different light sources, the reaction rates in different experiments can be compared on a basis of photonic efficiency or quantum yield [36,37]. Here, the photonic efficiency of reaction (ζ) is defined below:

$$\zeta = \frac{R}{I_0}$$

where R is the initial rate of 2,3-DCP degradation (mol L^{-1} min^{-1}) and I_0 is the incident photon flux (Einstein m^{-2} s^{-1}).

According to the conversion factors among radiation intensity, photon (energy) intensity, and lumination intensity [38], the values of ζ for different systems were calculated based on the above equation and are summarized in Table 2. In addition, a relative photonic efficiency (ζ_r) is also determined for easy comparison as listed in Table 2. It can be seen that the TNT film demonstrated the highest ζ value of 0.4037 (ζ_r = 1.0) under UV light irradiation, whereas it revealed much lower ζ value of 0.003 (ζ_r = 0.0074) under sunlight and had almost no activity under visible light irradiation. In the meantime, the photonic efficiency of PTh3/TNT under UV, sunlight and visible irradiation was determined to be 0.2243 (ζ_r = 0.556), 0.0046 (ζ_r = 0.0114) and 0.0036 (ζ_r = 0.0089), respectively. From the above data, the photonic efficiency of all systems can be ranked as UV/TNT > UV/PTh3/TNT > sun/PTh3/TNT > vis/PTh3/TNT > sun/TNT > vis/TNT. These results confirmed that the PTh/TNT catalyst demonstrated the higher photonic efficiency (ζ_r = 0.0114) than the TNT catalyst under

sunlight irradiation (ζ_r = 0.0074) due to its overall light absorption in a broad range of near UV and also visible region. It may imply that such composite catalysts could better utilize sunlight energy for its practical application in water and waster treatment.

[Table 2]

3.7. Effect of the side-chain substitution of polythiophene on photoactivity

Substitution patterns are strong features of polythiophenes and their derivatives, and significantly influence their physical, optical and electronical properties [39,40]. In principle, optimal polymer substitution should lead to an effective charge transfer without unwanted conformational changes, leading to good optical efficiency. In this study, three polythiophene derivatives with different side-chains, poly3-methylthiophene (P3Meth), poly3-hexylthiophene (P3Hexth), and polythiophenecarboxylic acid (PThCA), were electropolymerized on the TNT substrate and the effect of the side-groups on the 2,3-DCP degradation under visible light irradiation was investigated. The experimental results as listed in Table 3 show that the 2,3-DCP degradation with the P3Meth/TNT film was achieved by 52%, close to that with PTh3/TNT by 51%. In the meantime, the similar DOC removals in both experiments were achieved by > 26%. As compared to PTh3/TNT and P3Meth/TNT, the PThCA/TNT and P3Hexth/TNT catalysts exhibited the lower photocatalytic activity under the same experimental condition in terms of 2,3-DCP degradation and DOC removal significantly. It can be understood that the visible photoactivity of polymer/TNT composites is significantly dependent on the efficiency of light absorption by polymer as well as the electron transfer on the interface of polymer/TNT composites.

To increase the light harvest by catalysts, the strong and broad absorbance of light are both needed. Li and co-worker [41,42] have reported that thiophene polymers as electron-donor substituents with some side-chains such as the methoxy group can benefit the light absorption with a red shift, but the polymers with other side chains such as styryl and hexyl groups, due

to their large steric hindrance, may weaken the absorbance in the visible region [43]. In this study, the addition of methyl group in polymer backbone, due to its electron-donating ability, led to the red-shift absorption and enhanced its photoactivity as listed in Table 3. On the other hand, the steric hindrance of hexyl group weakened the interaction between the polymer chains and resulted in a less degree of 2,3-DCP degradation. A further reason is that the loading of P3Hexth onto TNT would reduce the pore volume and also surface area of the catalyst as supported by its FESEM result (The image is not provided here). This phenomenon was not observed in the images of P3Meth/TNT and PThCA/TNT. For the addition of carboxyl group, an electron-withdrawing subunit, the opposite trend in comparison to methyl group should be expected, as the mentioned above. While the positive effect may be compensated by the formation of coordination bands between polymer and TiO_2 nanotubes, which results from the esterification of carboxylic acid with hydroxylic groups on titania surface. There are a number of literature precedents suggesting that carboxylic acid and hydroxylic groups on oxide surface form chelates or coordinative bonds [44,45]. Taking into account these results, the possible coordination can be found in Scheme 2. In this way, a dramatic acceleration of the interfacial electron transfer from the conduction band of the polymer to TiO_2 acceptors is achieved. Therefore, it can infer that the side-chain structures of conjugated polymer have obvious influence on the photocatalytic activity of the polymer/TNT composites.

[Table 3]

4. Conclusions

In this study, polythiophene was successfully deposited on the TiO_2 nanotube films by a two-step electrochemical method. XPS spectra of PTh/TNT composites indicate the strong interaction between S sites of polymer backbone and TiO_2 nanotubes, in which electron

transfer from polythiophene to titania takes place. UV-vis DRS analysis shows that these composites have a strong photoresponse in the visible region at 500 nm. The prepared PTh/TNT films revealed significant activity for 2,3-DCP degradation under visible light irradiation and also sunlight irradiation, in which the PTh3/TNT film achieved the best performance. The experiments also confirmed that the side-chains of polythiophene could influence its photocatalytic activity significantly with an order of P3Meth/TNT ≈ PTh3/TNT > PThCA/TNT > P3Hexth/TNT. Further work is required to evaluate the effectiveness of this catalyst in degrading common pollutants and the reaction pathways under UV and visible illumination, respectively.

Acknowledgements

The authors wish to acknowledge the support of the Research Committee of The Hong Kong Polytechnic University in providing a PhD scholarship for H. C. Liang.

References

[1] J. Cao, J.Z. Sun, J. Hong, X.G. Yang, H.Z. Chen, M. Wang, Appl. Phys. Lett. 83 (2003) 1896-1898.

[2] K. Hara, K. Sayama, Y. Ohga, A. Shinpo, S. Suga, H. Arakawa, Chem. Commun. 2001, 569-570.

[3] A. Hagfeldt, M. Grätzel, Acc. Chem. Res. 33 (2000) 269-277.

[4] L.M. Peter, D.J. Riley, E.J. Tull, K.G.U. Wijayantha, Chem. Commun. 2002, 1030-1031.

[5] K. Kalyanasundaram, Coord. Chem. Rev. 46 (1982) 159-244.

[6] H. Rensmo, K. Westermark, S. Södergren, O. Kohle, P. Perssona, S. Lunell, H. Siegbahn, J. Chem. Phys. 111 (1999) 2744-2750.

[7] A. Pron, P. Rannou, Prog. Polym. Sci. 27 (2002) 135-190.

[8] S.E. Shaheen, C.J. Brabec, F. Padinger, T. Fromherz, J.C. Hummelen, N.S. Sariciftci, Appl. Phys. Lett. 78 (2001) 841-843.

[9] L.B. Roberson, M.A. Poggi, J. Kowalik, G.P. Smestad, L.A. Bottomley, L.M. Tolbert, Coordin. Chem. Rev. 248 (2004) 1491-1499.

[10] W.J.E. Beek, M.M. Wienk, M. Kemerink, X. Yang, R.A.J. Janssen, J. Phys. Chem. B 109 (2005) 9505-9516.

[11] S.X. Min, F. Wang, Y.Q. Han, J. Mater. Sci. 42 (2007) 9966-9972.

[12] U. Salzner, J.B. Lagowski, P.G. Pickup, R.A. Poirier, Synth. Met. 96 (1998) 177-189.

[13] J.H. Snook, L.A. Samuelson, J. Kumar, Y.G. Kim, J.E. Whitten, Org. Electron. 6 (2005) 55-64.

[14] W.R. Duncan, O.V. Prezhdo. Annu. Rev. Phys. Chem. 58 (2007) 143-184.

[15] C. Zafer, C. Karapire, N.S. Sariciftci, S. Icli, Sol. Energ. Mater. Sol. C. 88 (2005) 11-23.

[16] S. Yanagida, G.K.R. Senadeera, K. Nakamura, T. Kitamura, Y. Wada, J. Photochem. Photobiol. A 166 (2004) 75-80.

[17] C. Wen, K. Hasegawa, T. Kanbara, S. Kagaya, T. Yamamoto. J. Photochem. Photobiol. A 133 (2000) 59-66.

[18] B. Mukthaa, D. Mahantaa, S. Patila, G. Madras, J. Solid State Chem. 180 (2007) 2986-2989.

[19] L. Song, R.L. Qiu, Y.Q. Mo, D.D. Zhang, H. Wei, Y. Xiong, Catal. Commun. 8 (2007) 429-433.

[20] D.D. Eley, Chemistry Cationic Polymerization; P. H. Plesch, Ed., Macmillan, New York, 1963.

[21] W. Chen, G. Xue, Prog. Polym. Sci. 30 (2005) 783–811.

[22] X.Z. Li, F.B. Li, C.L. Yang, W.K. Ge, J. Photochem. Photobiol. A 141 (2001) 209-217.

[23] A.R. Hillman, E.F. Mallen, J. Electroanal. Chem. 220 (1987) 351-367.

[24] L.L. Miller, B. Zinger, Q.X. Zhou, J. Am. Chem. Soc. 109 (1987) 2267-2272.

[25] The Southampton Electrochemistry Group, Instrumental Methods in Electrochemistry, Ellis Horwood, Chichester, 1985, p. 283.

[26] O.K. Varghese, D. Gong, M. Paulose, C.A. Grimes, E.C. Dickey, J. Mater. Res. 18 (2003) 156-165.

[27] D. Eder, I.A. Kinloch, A.H. Windle, Chem. Commun. 2006, 1448-1450.

[28] S. Takemura, H. Kato, Y. Nakajima, Appl. Surf. Sci. 144-145 (1999) 360-365.

[29] Q.T. Vu, M. Pavlik, N. Hebestreit, J. Pfleger, U. Rammelt, W. Plieth, Electrochim. Acta 51 (2005) 1117-1124.

[30] Y.Q. Gou, D.Y. Chen, Z.X. Su, Appl. Catal. A 261 (2004) 15-18.

[31] K. Demeestere, J. Dewulf, T. Ohno, P.H. Salgado, H.V. Langenhove, Appl. Catal. B 61 (2005) 140-149.

[32] H. Park, W. Choi, J. Phys. Chem. B 109 (2005) 11667-11674.

[33] W.S. Kuo, P.H. Ho, Dyes Pigments 71 (2006) 212-217.

[34] E.R. Bandala, S. Gelover, M.T. Leal, C.A. Bulnes, A. Jimenez, C.A. Estrada, Catal. Today 76 (2002) 189-199.

[35] W. C. Hao, F. Pan, T. M. Wang, J. Mater. Sci. 40 (2005) 1251-1253.

[36] N. Serpone, R. Terzian, D. Lawless, P. Kennepohl. G. Sauve, J. Phoiochem. Photobiol. A 73 (1993) 11-16.

[37] N. Serpone, J. Adv. Oxid. Technol. 2 (1997) 203-216.

[38] R.W. Thimijan, R.D. Heins, Hortscience 18 (1983) 818-822.

[39] H.Y. Li, A. Sundararaman, K. Venkatasubbaiah, F. Jäkle, J. Am. Chem. Soc. 129 (2007) 5792-5793.

[40] G. Vamvounis, J.F. Yu, S. Holdcroft, Eur. Polym. J. 40 (2004) 2659-2664.

[41] Z.A. Tan, E.J. Zhou, Y. Yang, Y.J. He, C.H. Yang, Y.F. Li, Eur. Polym. J. 43 (2007) 855-861.

[42] J.H. Hou, L.H. Huo, C. He, C.H. Yang, Y.F. Li, Macromolecules 39 (2006) 594-603.

[43] N. Somanathan, S. Radhakrishnan, Int. J. Mod. Phys. B 19 (2005) 4645-4676.

[44] H. Frei, D.J. Fitzmaurice, M. Grätzel, Langmuir 6 (1990) 198-206.

[45] J. Moser, S. Punchihewa, P.P. Infelta, M. Grätzel, Langmuir 7 (1991) 3012-3018.

List of figure captions

Fig. 1. Schematic diagram of conjugated polymer/TNT nanocomposites; detailed view on the polymer-TiO_2 junction and free charge carrier photogeneration mechanism is shown. Here, the conjugated polymer denotes as polythiophene in present paper.

Fig. 2. Field-emission scanning electron microscopy (FESEM) images of TNT and its composites: (a1) TNT, (b1) PTh1/TNT, (c1) PTh3/TNT, and (d1) PTh5/TNT; (a2), (b2), (c2) and (d2) are their corresponding EDX spectra, respectively.

Fig. 3. The current density-time transients for the polymerization of thiophene under constant potential of 1.3 V. Curves a, b, and c corresponding to 1 mM, 3 mM, and 5 mM thiophene in BFEE solution, respectively.

Fig. 4. XRD patterns of Ti foil, pure TNT, and PTh/TNT composite films.

Fig. 5. (a) High resolution S 2p spectra of pure PTh and PTh/TNT composites; (b) Ti 2p spectra of pure TNT film and PTh/TNT composites. Dot line: experimental curve; Solid line: deconvolution curve. (The high resolution XPS spectrum of PTh1/TNT was not listed here due to the too small amount of S/Ti, which could cause an inaccurate data).

Fig. 6. (1) UV-Vis absorption spectrum of PTh/ITO (curve a); (2) The diffuse reflectance spectra of a pure TNT and polythiophene modified TNT samples (curve b, c, d, and e represents the spectrum of TNT, PTh1/TNT, PTh3/TNT, PTh5/TNT, respectively).

Fig. 7. (a) The direct vis-photolysis process (■), photocatalysis of catalyst TNT (●) and PTh3/TNT (▲) of 2,3-DCP in aqueous solutions; (b) The degradation of 2,3-DCP by photocatalytic technology with the PTh/TNT composites (PTh1/TNT: ▼; PTh3/TNT: ▲; PTh5/TNT: ◄). Here, $[C_o]$ = 20 mg L^{-1} and all the plotted curves were calibrated by the evaporation of 2,3-DCP in the dark.

Fig. 8. Photodegradation of 2,3-DCP solution in the presence of different systems under UV irradiation (a 8W-UV lamp with 365 nm). Here $[C_o]$ = 20 mg L^{-1} and all the plotted curves were calibrated by the evaporation of 2,3-DCP in the dark.

Fig. 9. Photodegradation of 2,3-DCP solution in the presence of TNT and PTh3/TNT under sunlight. Here, $[C_o]$ = 20 mg L^{-1} and the evaporation of 2,3-DCP during reaction has been deducted according to the results of a blank experiment without catalyst.

Table 1

Binding energy of TNT, PTh and PTh/TNT samples in XPS analysis

Sample	Ti $2p_{3/2}$ [eV]	Ti $2p_{1/2}$ [eV]	S $2p_{3/2}$ [eV]	S $2p_{1/2}$ [eV]
TNT	459.48	465.17	–	–
PTh	–	–	163.32	164.41
			167.57	
PTh3/TNT	459.15	464.83	163.69	164.89
			168.28	
PTh5/TNT	458.88	464.56	163.58	164.74
			167.82	

Table 2

Comparison of rate constant, photonic efficiency, and relative photonic efficiency of different systems for the degradation of 2,3-DCP (20 mg L^{-1} = 0.123 mmol L^{-1}).

Studied system[a]	2,3-DCP degradation[b] (C_0 = 0.123 mmol L^{-1})			
	k ($\times 10^{-3}$ min^{-1})	R ($\times 10^{-5}$ mmol L^{-1} min^{-1})	ζ (mol $Einstein^{-1}$ m^{-1})	ζ_r
TNT + UV	5.4	66.42	0.4037	1.0000
PTh3/TNT + UV	3.0	36.90	0.2243	0.5560
TNT + vis	--[c]	--	--	--
PTh3/TNT + vis	1.7	20.91	0.0036	0.0089
TNT + sun	2.7	33.21	0.0030	0.0074
PTh3/TNT + sun	4.1	50.43	0.0046	0.0114

[a] In the studied systems, the light intensity of UV, visible, and sunlight is 27.42, 978.07, and 1832.57 μ Einstein m^{-2} s^{-1}, respectively.

[b] The 2,3-DCP degradation is suggested to follow the pseudo-first order reaction and the reaction rate can be calculated from the equation: $R = k C_0$.

[c] -- is nearly zero.

Table 3

2,3-DCP degradation and DOC removal by different polymer/TNT composites

Sample	2,3-DCP degradation [%]	DOC removal [%]
PTh3/TNT	52	26.6
P3Meth/TNT	51	26.5
P3Hexth/TNT	34	9.6
PThCA/TNT	41	16.8

Fig. 1

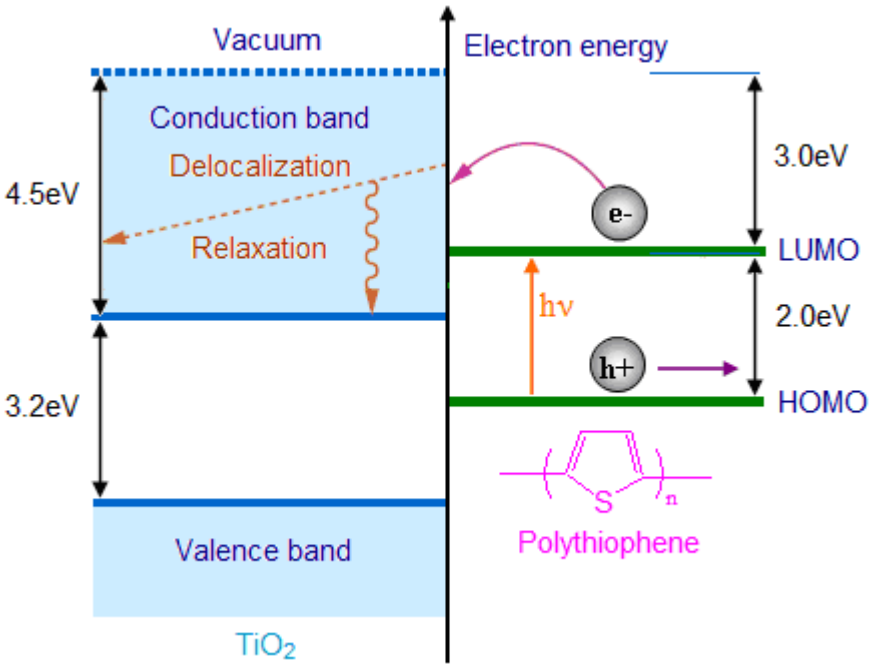

(The color figure is intended to be reproduced in black-and-white.)

Fig. 2

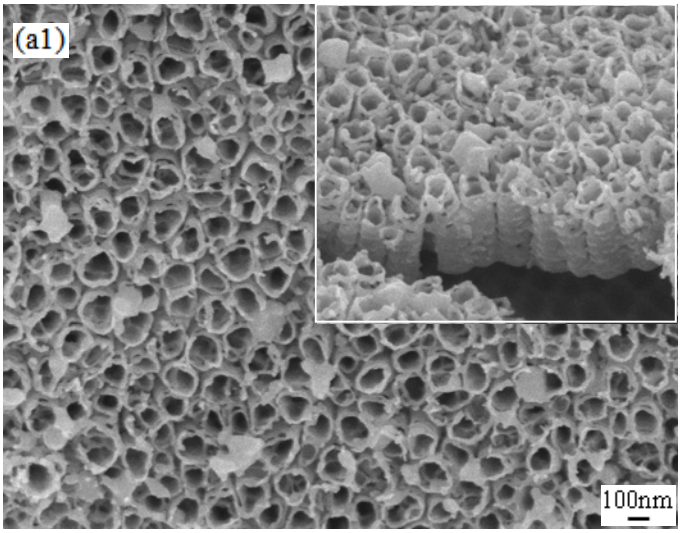
(a1)
100nm

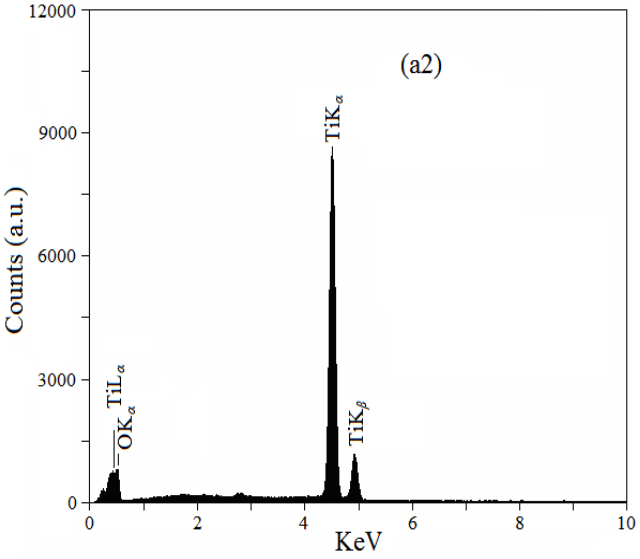
(a2)
Counts (a.u.)
KeV
TiK$_\alpha$
TiL$_\alpha$
OK$_\alpha$
TiK$_\beta$

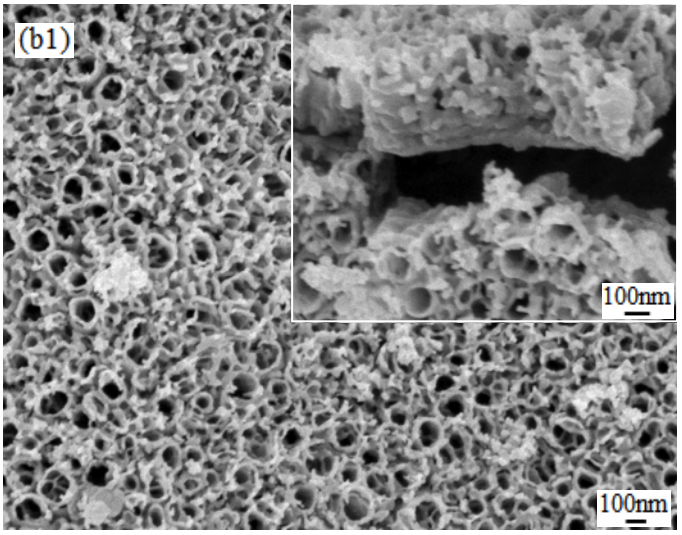
(b1)
100nm
100nm

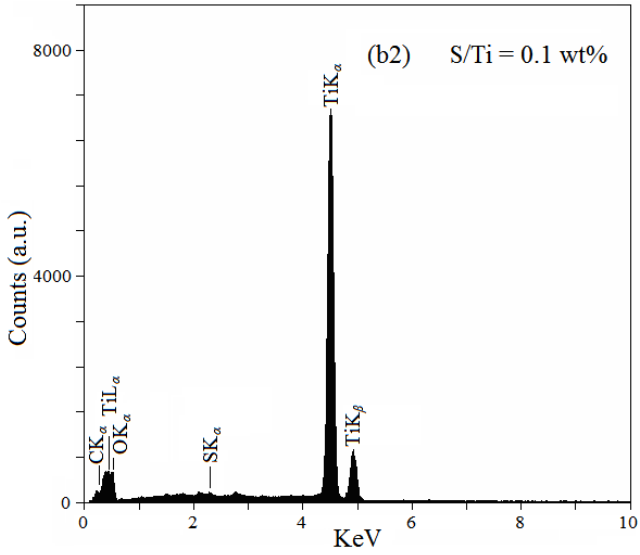
(b2)
S/Ti = 0.1 wt%
Counts (a.u.)
KeV
TiK$_\alpha$
CK$_\alpha$
TiL$_\alpha$
OK$_\alpha$
SK$_\alpha$
TiK$_\beta$

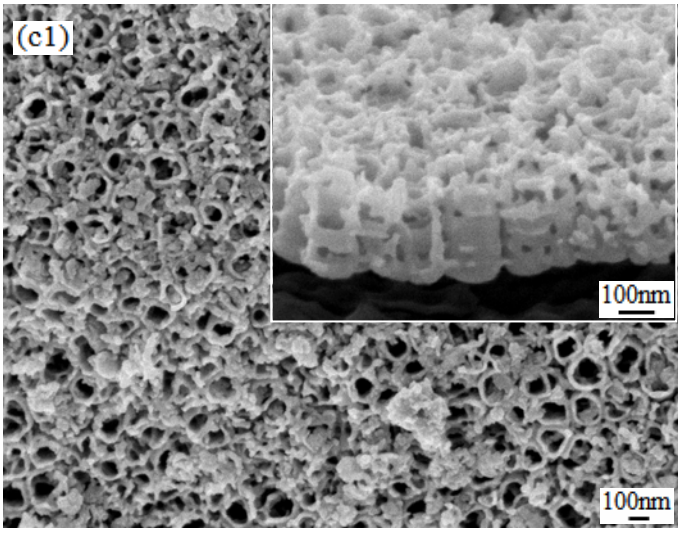
(c1)
100nm
100nm

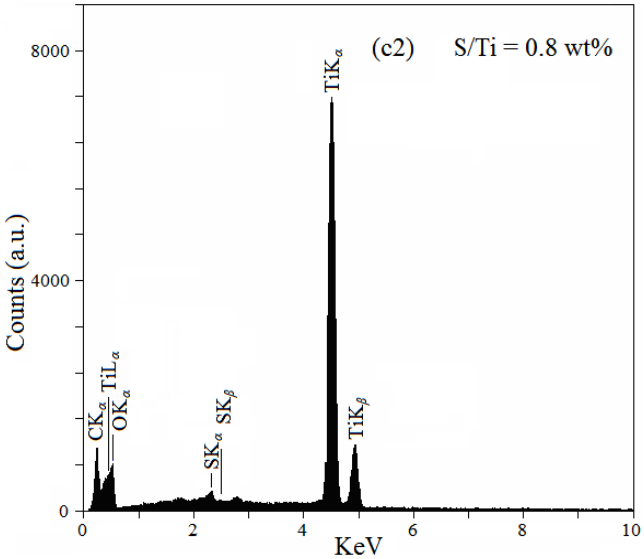
(c2)
S/Ti = 0.8 wt%
Counts (a.u.)
KeV
TiK$_\alpha$
CK$_\alpha$
TiL$_\alpha$
OK$_\alpha$
SK$_\alpha$
SK$_\beta$
TiK$_\beta$

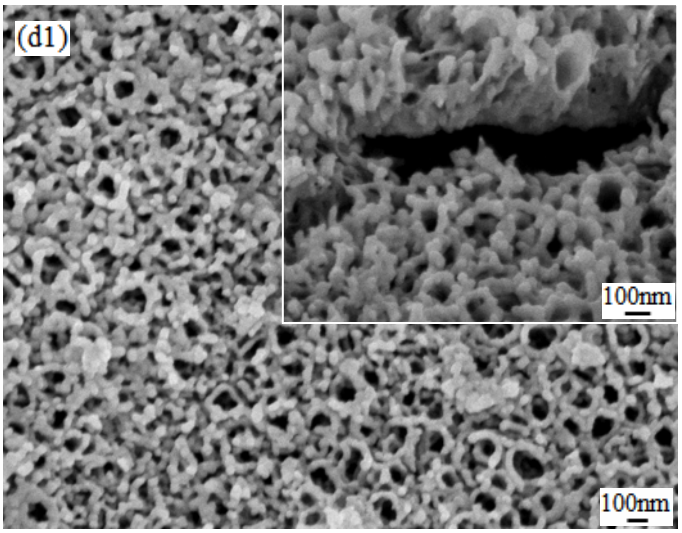
(d1)
100nm
100nm

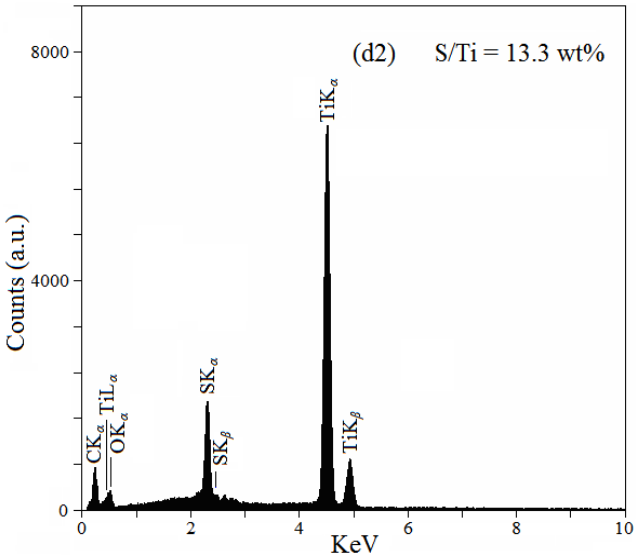
(d2)
S/Ti = 13.3 wt%
Counts (a.u.)
KeV
CKα
TiLα
OKα
SKα
SKβ
TiKα
TiKβ
0
4000
8000
0
2
4
6
8
10

Fig. 3

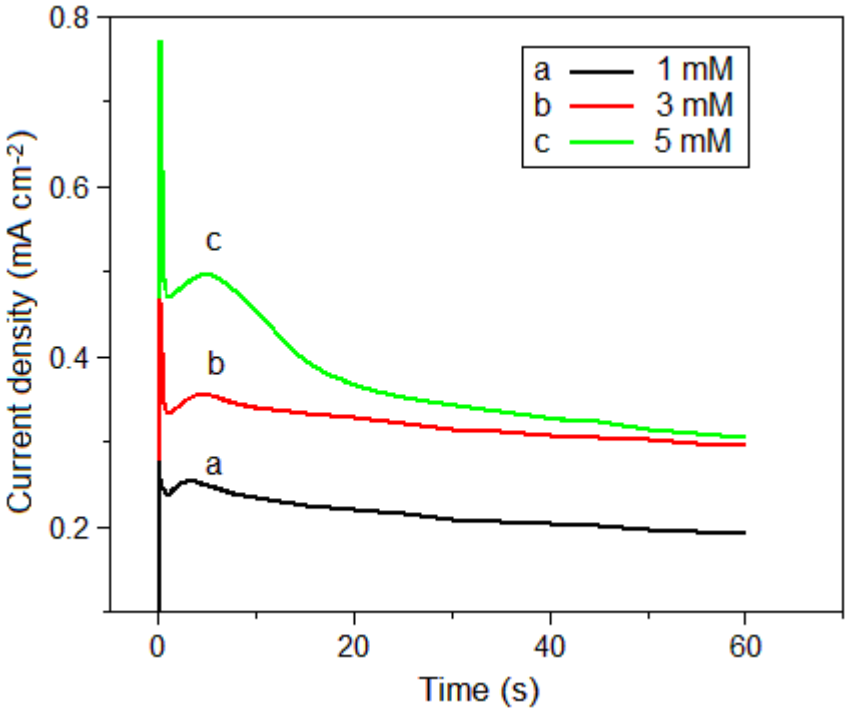

(The color figure is intended to be reproduced in black-and-white.)

Fig. 4

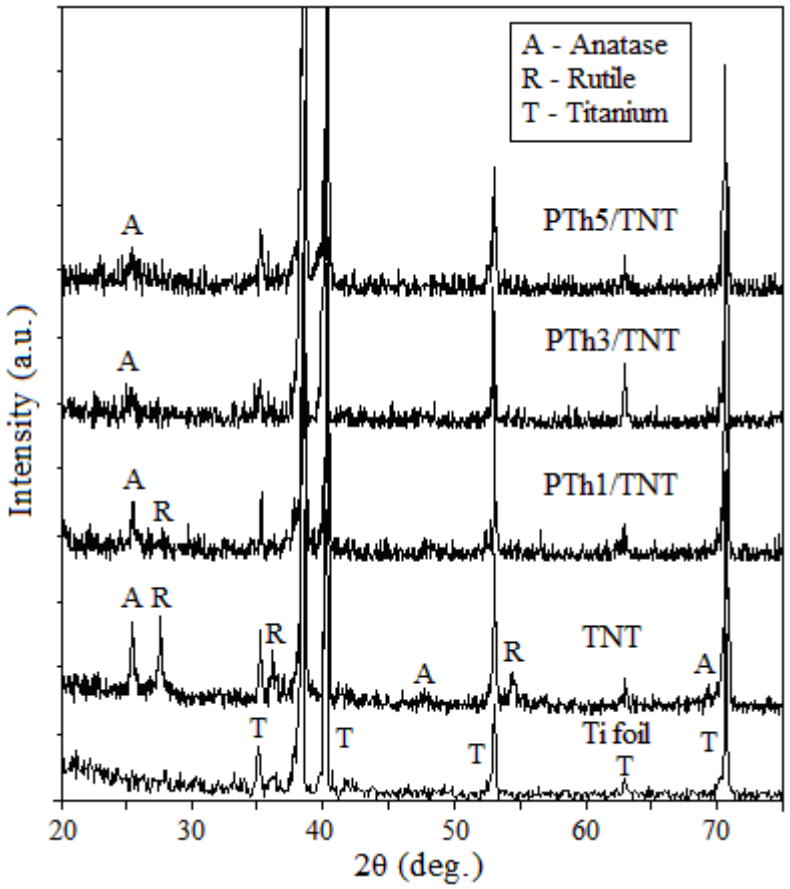
A - Anatase
R - Rutile
T - Titanium
PTh5/TNT
PTh3/TNT
PTh1/TNT
TNT
Ti foil
Intensity (a.u.)
2θ (deg.)
20
30
40
50
60
70

Fig. 5

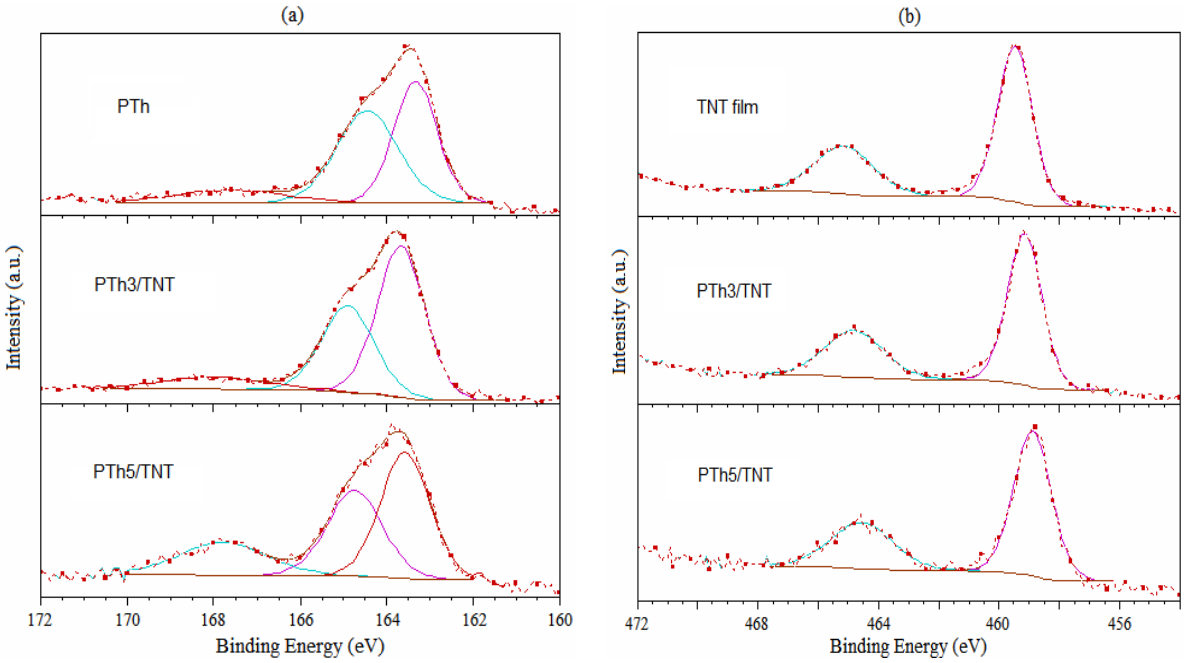

(The color figure is intended to be reproduced in black-and-white.)

Fig. 6

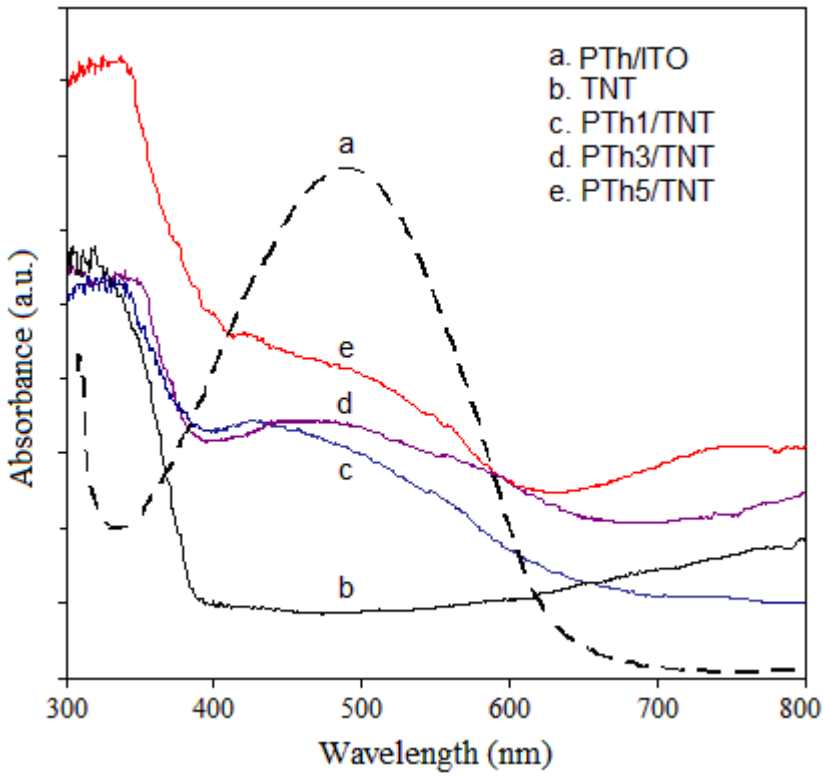

(The color figure is intended to be reproduced in black-and-white.)

Fig. 7

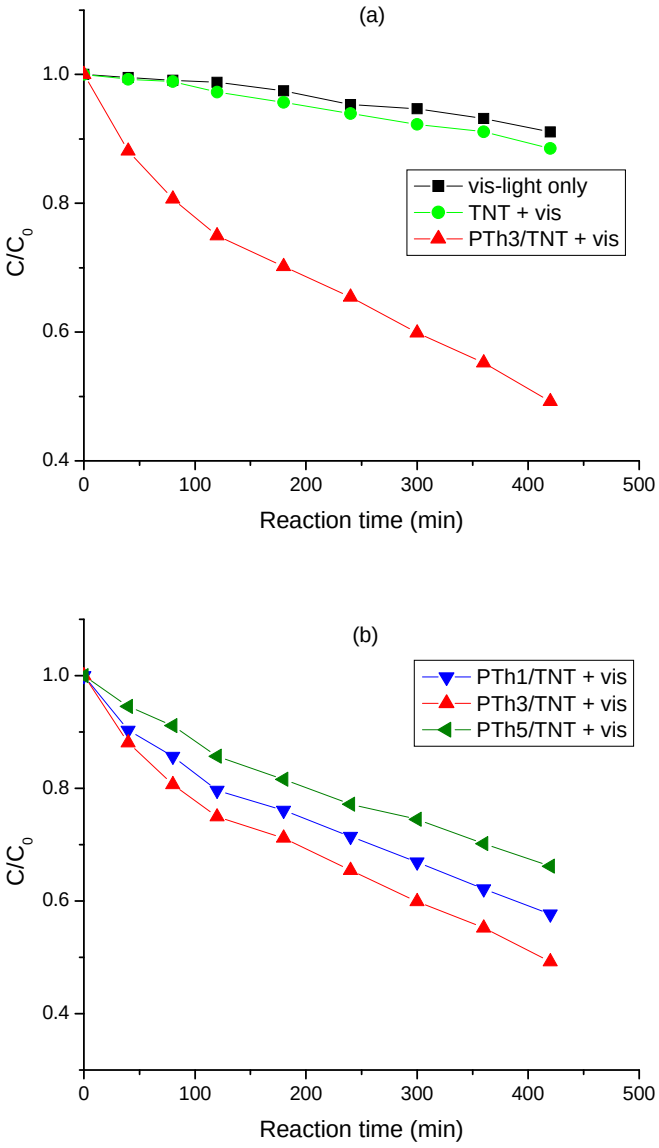

(The color figure is intended to be reproduced in black-and-white.)

Fig. 8

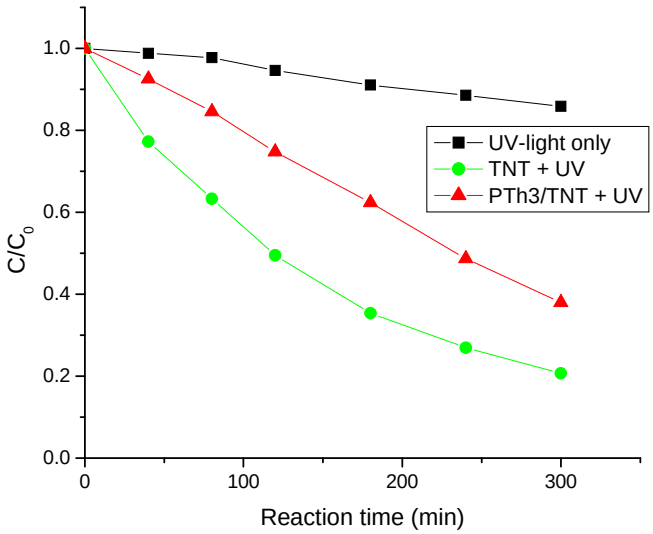

(The color figure is intended to be reproduced in black-and-white.)

Fig. 9

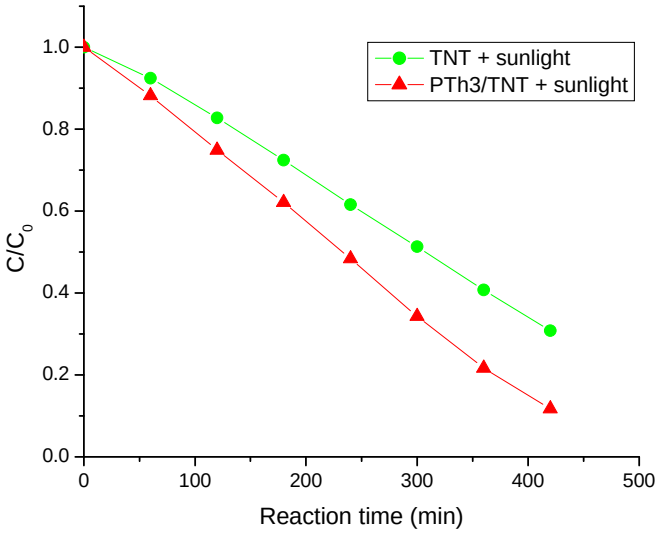

(The color figure is intended to be reproduced in black-and-white.)

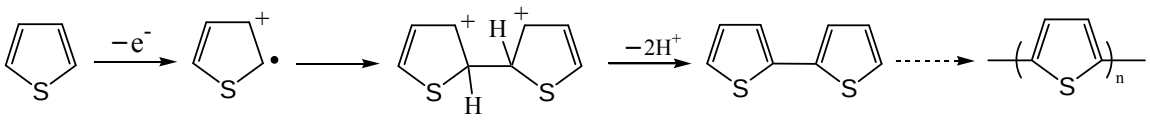

Scheme 1

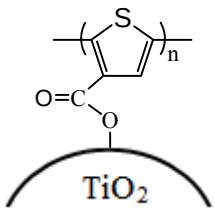

Scheme 2